

Supplement of Atmos. Chem. Phys., 16, 1637–1651, 2016
<http://www.atmos-chem-phys.net/16/1637/2016/>
doi:10.5194/acp-16-1637-2016-supplement
© Author(s) 2016. CC Attribution 3.0 License.



Atmospheric
Chemistry
and Physics
Open Access
EGU

Supplement of

Size-resolved measurements of ice-nucleating particles at six locations in North America and one in Europe

R. H. Mason et al.

Correspondence to: A. K. Bertram (bertram@chem.ubc.ca)

The copyright of individual parts of the supplement might differ from the CC-BY 3.0 licence.

S1 Corrections used in calculating INP number concentrations with the MOUDI-DFT

As the DFT analyses only a small fraction of the entire sample, the number of INPs identified through droplet freezing must be extrapolated to the entire sample. Within a MOUDI sample, the deposit is not uniform and the particle concentration varies with position, and this must be taken into account in the extrapolation. Used in Equations (1) and (2) of the main text, respectively, $f_{\text{nu},0.25-0.10\text{mm}}$ accounts for deposit non-uniformity within the microscope viewing area of the droplet freezing technique and $f_{\text{nu},1\text{mm}}$ accounts for deposit non-uniformity across the entire sample. Values are reported in Table S1.

The DFT relies on a relatively small number of nucleation events (34.8 on average). Koop et al. (1997) calculate a statistical uncertainty at a fixed confidence level associated with a given number of number of observed nucleation events. The values of f_{ne} , defined as $\omega t_{\text{tot}}/n_{\text{nuc}}$ in Koop et al. (1997) where ω is the nucleation rate, t_{tot} is the observation time, and n_{nuc} is the number of nucleation events, were calculated using equations 10a and 10b of Koop et al. (1997). While Koop et al. (1997) used a confidence level of 99.9 % (values in Table 2 of the Appendix in that paper), here we use a confidence level of 95 %.

S2 Calculations of fractions of INPs larger than 1, 1.2, or 2.5 μm from previous studies

S2.1 Rucklidge (1965)

An INP size distribution was reported in Fig. 6 of Rucklidge (1965) for sampling conducted at a site 11 miles east of West Plains, Missouri. The INP distribution was given for sizes ranging from 0.1–3.1 μm , and from this the fraction of the total ice crystals containing INPs larger than 1 μm was calculated. Given that the INP was assumed to be the largest particle but, in some cases, smaller particles were also present, we report the fraction of INPs $> 1 \mu\text{m}$ as an

upper limit. Rucklidge (1965) used an expansion chamber in this study, giving ice nucleation temperatures between -12 and -25 °C.

S2.2 Vali (1966)

The size distribution of INPs found in hail melt water was reported by Vali (1966). Hail from Alberta, Canada was melted and some of this water was passed through filters of either 0.01 or 1.2 µm pore size. Samples were then analyzed using a drop freezing method. The concentration of INPs in the immersion mode as a function of temperature was given in Fig. 3 of that study for three size ranges: unfiltered, 1.2 µm filtered, and 0.01 µm filtered hail melt water. To calculate the fraction of INPs > 1.2 µm at -12.8 °C (the lowest temperature available and therefore the closest to -15 °C), the concentration of INPs in the 1.2 µm-filtered sample was first divided by the concentration of INPs in the unfiltered sample at this temperature. This fraction was then subtracted from unity.

Only the sample of Vali (1966) underwent size-segregation by filtration. We note that the suspension of particles in an aqueous system during the size-selection process may affect the surface properties of the particle, and therefore it's ability to nucleate ice. If suspension results in the dissolution of soluble components or facilitates the breakup of aggregated components, this may reduce the size of INPs. On the other hand, coagulation of particles upon suspension could increase the INP size.

S2.3 Rosinski et al. (1986)

The size distributions of INPs active in the immersion and condensation nucleation modes over the central and western South Pacific Ocean were determined by Rosinski et al. (1986). Aerosol particle samples were size-selected by an Anderson cascade impactor (similar in

principle to the MOUDI) where the stage size cuts were 8, 6, 5, 4, 1, and 0.5 μm . There were also two after filters connected to the impactor in parallel to collect particles smaller than 0.5 μm . Samples were analyzed using either the drop freezing method (immersion mode) or a dynamic developing chamber (condensation mode).

Immersion mode freezing data for twelve samples was reported in Tables 1–12 of Rosinski et al. (1986) with each table corresponding to a different sampling period. As filter measurements were not reported for all samples and it is unclear whether differences in the size of deposits between the impactor and filter samples was accounted for during immersion freezing measurements, here we focus on the impactor samples for the immersion freezing data. We also assume that the freezing of a drop was caused by the presence of a single INP. The fraction of INPs $> 1 \mu\text{m}$ was calculated for each sample in 0.1 $^{\circ}\text{C}$ intervals, and these values were then averaged over all samples. The average fraction of INPs $> 1 \mu\text{m}$ is reported at -10.8 $^{\circ}\text{C}$. Values are not reported at lower temperatures because of sample saturation.

Condensation mode freezing data was reported in Table 13 of Rosinski et al. (1986). Samples V–VII and IX–XI were used here as these report INP concentrations for all impactor stages, one after filter, and for particles $> 1 \mu\text{m}$. Although not reported in Table 13, the INP concentrations on the second after filter are assumed to equal those found on the first after filter as instructed in the text. INP concentrations missing from Table 13 were calculated by linear interpolation where possible. The fraction of INPs $> 1 \mu\text{m}$ was first determined for each sample in 1 $^{\circ}\text{C}$ intervals, and then averaged over all samples. The average fraction of INPs $> 1 \mu\text{m}$ is reported at -5 to -6 $^{\circ}\text{C}$ as this is the lowest temperature where data is available for all particle sizes in all samples.

S2.4 Rosinski et al. (1988)

Rosinski et al. (1988) measured the INP size distribution over the Gulf of Mexico by first size selecting aerosol particles with an Andersen cascade impactor with after filters and then analyzing these samples with a dynamic developing chamber. Five size cuts were used for size selection: > 4.5 , 3.1 , 1.0 , 0.4 , and $0.1 \mu\text{m}$. Figures 2 and 5–7 of that study presented INP concentrations for the condensation freezing mode in twenty samples.

The fraction of INPs $> 1 \mu\text{m}$ was determined in $1 \text{ }^\circ\text{C}$ intervals within each sample, and then averaged over all samples. In this analysis, sample 1 from August 6, 1986 was excluded as data was missing for particle sizes $> 3.1 \mu\text{m}$. The average fraction of INPs $> 1 \mu\text{m}$ is reported over -15 to $-16 \text{ }^\circ\text{C}$. Values were not calculated for lower temperatures due to sample saturation.

S2.5 Berezinski et al. (1988)

The size distribution of INPs active in the condensation nucleation mode over Eastern Europe was determined by Berezinski et al. (1988). Aerosol particle samples were first collect by a cascade impactor with size cuts of 100 , 30 , 10 , 1.0 , and $0.1 \mu\text{m}$ and then analyzed using a thermal diffusion chamber and microscope. Data is presented in Table 1 of that study at freezing temperatures of -8 , -10 , -12 , -15 , and $-20 \text{ }^\circ\text{C}$. Data was used directly from Table 1 to determine the average fraction of INPs $> 1 \mu\text{m}$. To match the conditions used in this study, the average fraction of INPs $> 1 \mu\text{m}$ is reported for temperatures of -15 and $-20 \text{ }^\circ\text{C}$.

S2.6 Mertes et al. (2007)

Using a counterflow virtual impactor designed for the collection of atmospheric ice particles, in this case for ice crystal sizes of 5 – $20 \mu\text{m}$, Mertes et al. (2007) determined the sizes of ice crystal residuals from mixed-phase clouds at the high alpine research station of

Jungfrauoch in Switzerland. Data is presented in Fig. 9 of Mertes et al. (2007) for particles sizes between 20 nm and 5 μm , and this was used to calculate the fraction of the ice crystal residuals that were $> 1 \mu\text{m}$ in size. The temperature at time of collection was on average $-17.4 \text{ }^\circ\text{C}$.

S2.7 Santachiara et al. (2010)

Santachiara et al. (2010) collected size-resolved aerosol samples on filters by passing ambient air through various sampling heads with size cut-points of either 1, 2.5, or 10 μm . The total suspended particulate was also collected. Aerosol particle samples were then analyzed in a dynamic developing chamber to determine the concentration of INPs active in the condensation mode of freezing. Table 3 of that study presented the fractions of INPs < 1 and $< 2.5 \mu\text{m}$, which were subtracted from unity here. We report the averaged values between -17 and $-19 \text{ }^\circ\text{C}$.

S2.8 Huffman et al. (2013)

The size distribution of INPs at a forest site in Colorado was measured by Huffman et al. (2013) using an early iteration of the MOUDI-DFT used in this study. Figure 4 of that study presented INP concentrations as a function of size, which we used to calculate the average fraction of INPs $> 1 \mu\text{m}$. As was done in Huffman et al. (2013), INP values are reported separately for samples collected during rainfall and samples collected during dry weather. We report the average fraction of INPs $> 1 \mu\text{m}$ at -15 to $-20 \text{ }^\circ\text{C}$ for both sampling conditions.

S2.9 Other studies

Additional studies reporting INP sizes have not been included here are Bigg and Hopwood (1963), because INP size was calculated based on several assumptions that were not confirmed, and Rosinski et al. (1987), because only the onset freezing temperature was given for each experiment.

References

- Berezinski, N. A., Stepanov, G. V. and Khorguani, V. G.: Ice-forming activity of atmospheric aerosol particles of different sizes, *Lecture Notes in Physics*, edited by P. E. Wagner and G. Vali, 309, 709–712, 1988.
- Bigg, E. K. and Hopwood, S. C.: Ice Nuclei in the Antarctic, *J. Atmos. Sci.*, 20, 185–188, 1963.
- Huffman, J. A., Prenni, A. J., DeMott, P. J., Pöhlker, C., Mason, R. H., Robinson, N. H., Fröhlich-Nowoisky, J., Tobo, Y., Després, V. R., Garcia, E., Gochis, D. J., Harris, E., Müller-Germann, I., Ruzene, C., Schmer, B., Sinha, B., Day, D. A., Andreae, M. O., Jimenez, J. L., Gallagher, M., Kreidenweis, S. M., Bertram, A. K. and Pöschl, U.: High concentrations of biological aerosol particles and ice nuclei during and after rain, *Atmos. Chem. Phys.*, 13, 6151–6164, doi:10.5194/acp-13-6151-2013, 2013.
- Koop, T., Luo, B., Biermann, U. M., Crutzen, P. J. and Peter, T.: Freezing of HNO₃/H₂SO₄/H₂O solutions at stratospheric temperatures: Nucleation statistics and experiments, *J. Phys. Chem. A*, 101, 1117–1133, doi:10.1021/jp9626531, 1997.
- Mertes, S., Verheggen, B., Walter, S., Connolly, P., Ebert, M., Schneider, J., Bower, K. N., Cozic, J., Weinbruch, S., Baltensperger, U. and Weingartner, E.: Counterflow Virtual Impactor Based Collection of Small Ice Particles in Mixed-Phase Clouds for the Physico-Chemical Characterization of Tropospheric Ice Nuclei: Sampler Description and First Case Study, *Aerosol Sci. Technol.*, 41, 848–864, doi:10.1080/02786820701501881, 2007.
- Rosinski, J., Haagenson, P. L., Nagamoto, C. T. and Parungo, F.: Ice-forming nuclei of maritime origin, *J. Aerosol Sci.*, 17, 23–46, doi:10.1016/0021-8502(86)90004-2, 1986.
- Rosinski, J., Haagenson, P. L., Nagamoto, C. T. and Parungo, F.: Nature of ice-forming nuclei in marine air masses, *J. Aerosol Sci.*, 18, 291–309, doi:10.1016/0021-8502(87)90024-3, 1987.
- Rosinski, J., Haagenson, P. L., Nagamoto, C. T., Quintana, B., Parungo, F. and Hoyt, S. D.: Ice-forming nuclei in air masses over the Gulf of Mexico, *J. Aerosol Sci.*, 19, 539–551, doi:10.1016/0021-8502(88)90206-6, 1988.
- Rucklidge, J.: The Examination by Electron Microscope of Ice Crystal Nuclei from Cloud Chamber Experiments, *J. Atmos. Sci.*, 22, 301–308, 1965.
- Santachiara, G., Di Matteo, L., Prodi, F. and Belosi, F.: Atmospheric particles acting as Ice Forming Nuclei in different size ranges, *Atmos. Res.*, 96, 266–272, doi:10.1016/j.atmosres.2009.08.004, 2010.
- Vali, G.: Sizes of Atmospheric Ice Nuclei, *Nature*, 212, 384–385, doi:10.1038/212384a0, 1966.

Table S1. Deposit diameters, total area of the sample deposit (A_{deposit}), and non-uniformity correction factors, $f_{\text{nu},0.25-0.10\text{mm}}$ and $f_{\text{nu},1\text{mm}}$ for use in Equations (1) and (2), respectively, of the main text. The uncertainty in $f_{\text{nu},1\text{mm}}$ is given at 95 % confidence level.

MOUDI stage	Deposit diameter (mm)	A_{deposit} (mm ²)	$f_{\text{nu},0.25-0.10\text{mm}}$	$f_{\text{nu},1\text{mm}}$ with uncertainty
2*	23.25	424.6	$0.1225\exp(-11.29\mu) + 1.065\exp(-0.06412\mu)**$ $0.6505\exp(-7.33\mu) + 1.234\exp(-0.2126\mu)$	0.74, +0.20, -0.13 3.18, +0.38, -1.03
3*	26.25	541.2	$0.04718\exp(-14.15\mu) + 1.023\exp(-0.02347\mu)$	0.72, +0.08, -0.08 0.65, +0.03, -0.07
4	26.25	541.2	$0.04252\exp(-13.06\mu) + 1.024\exp(-0.02386\mu)$	1.18, +0.10, -0.15
5	26.25	541.2	$0.03023\exp(-14.97\mu) + 1.015\exp(-0.01515\mu)$	0.97, +0.03, -0.10
6	27.75	604.8	$0.5799\exp(-10.57\mu) + 1.148\exp(-0.1408\mu)$	0.75, +0.19, -0.02
7	27.25	583.2	$0.1151\exp(-10.66\mu) + 1.072\exp(-0.07029\mu)$	0.84, +0.07, -0.11
8	27.25	583.2	$1.03\exp(-12.79\mu) + 1.268\exp(-0.2422\mu)$	1.01, +0.03, -0.12

*Slight modifications to particle collection in MOUDI stages 2 and 3 were made between sampling at different locations, giving different values for $f_{\text{nu},0.25-0.10\text{mm}}$ and $f_{\text{nu},1\text{mm}}$.

** $\mu = N_u(T)/N_o$, where $N_u(T)$ is the number of unfrozen droplets at temperature T in the freezing experiment and N_o is the total number of droplets in the freezing experiment.

Table S2. The correction factor f_{ne} , which is a statistical uncertainty, derived for a given number of detected nucleation events with fewer nucleation events leading to a greater statistical uncertainty. Values were calculated at a confidence level of 0.95 based on the work of Koop et al. (1997).

Number of droplet freezing events	f_{ne} lower limit	f_{ne} upper limit
1	0.051	4.744
2	0.178	3.148
3	0.273	2.585
4	0.342	2.288
5	0.394	2.103
6	0.436	1.974
7	0.469	1.878
8	0.498	1.804
9	0.522	1.745
10	0.543	1.696
11	0.561	1.655
12	0.577	1.620
13	0.592	1.590
14	0.605	1.563
15	0.616	1.540
16	0.627	1.519
17	0.637	1.500
18	0.646	1.483
19	0.655	1.467
20	0.663	1.453
25	0.695	1.397
30	0.720	1.356
35	0.739	1.326
40	0.755	1.302
45	0.768	1.282
50	0.779	1.266
55	0.789	1.252
60	0.798	1.240
65	0.805	1.229
70	0.812	1.220
75	0.818	1.212
80	0.823	1.204

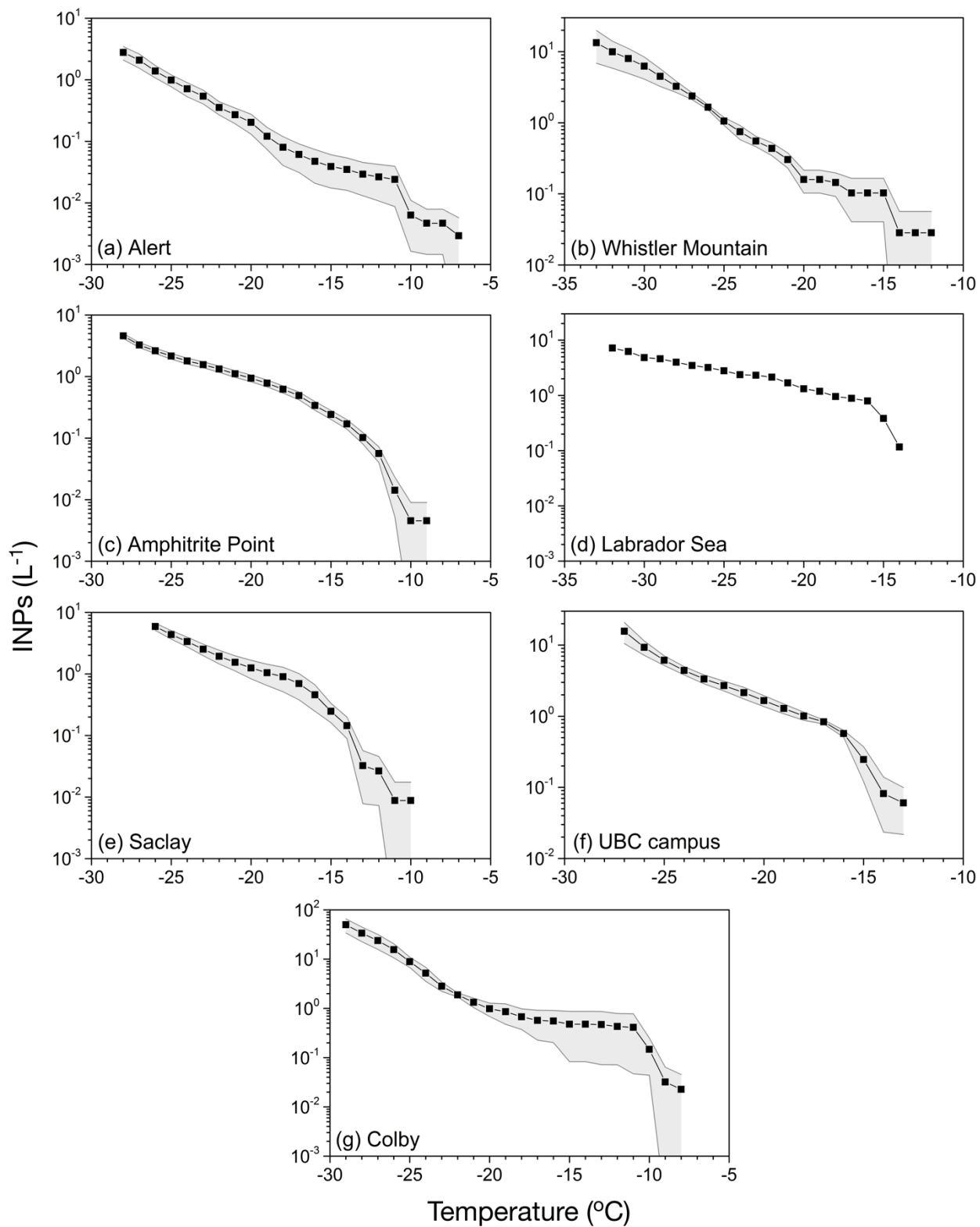


Figure S1. INP number concentrations as a function of temperature at each field site, averaged over all available samples. Uncertainty (shaded region) is given as the standard error of the mean. There is no uncertainty for the Labrador Sea sample as only a single sample was available.

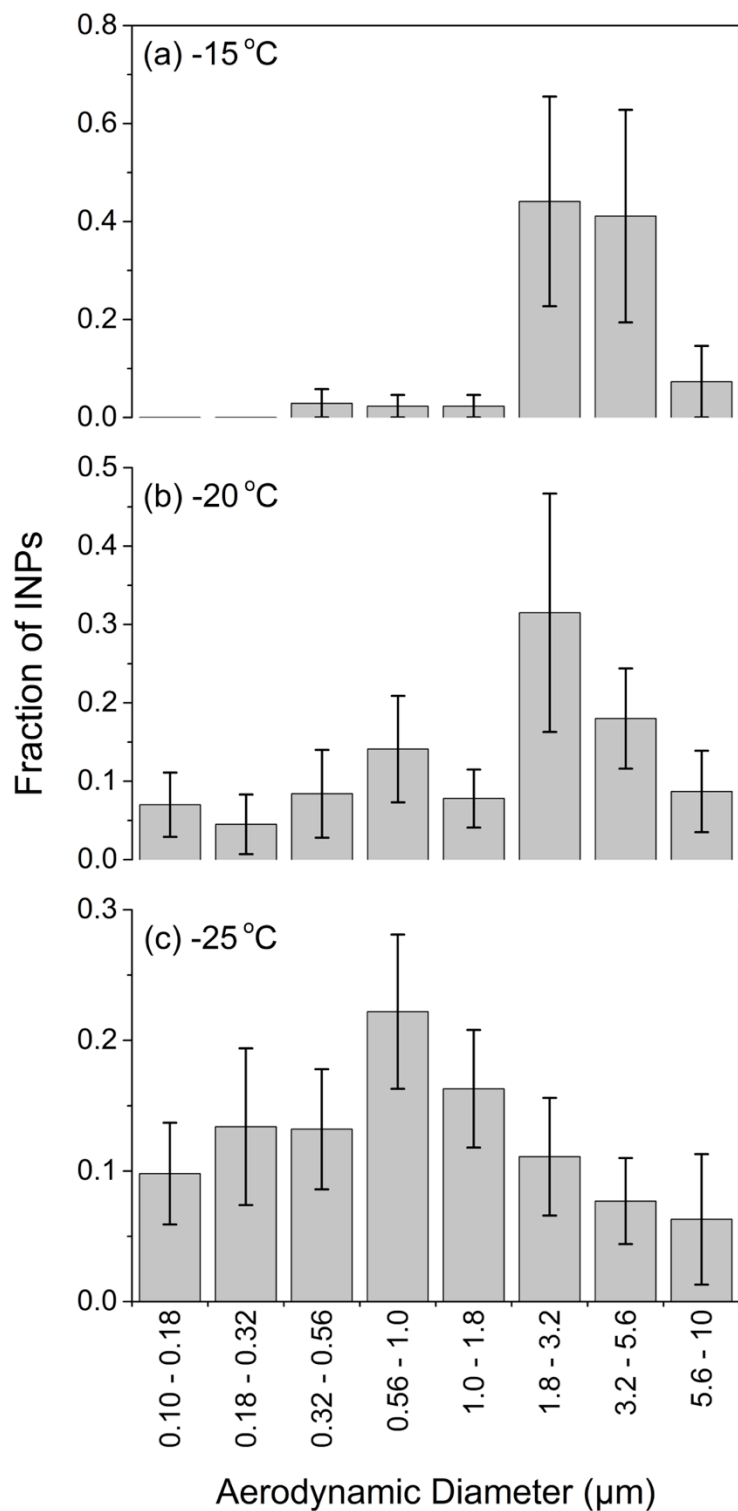


Figure S2. Mean INP size distributions at Alert, NU, Canada at (a) -15 $^{\circ}\text{C}$, (b) -20 $^{\circ}\text{C}$, and (c) -25 $^{\circ}\text{C}$. Here we report the fraction of INPs in each MOUDI size bin as the mean of all samples with uncertainty as the standard error of the mean.

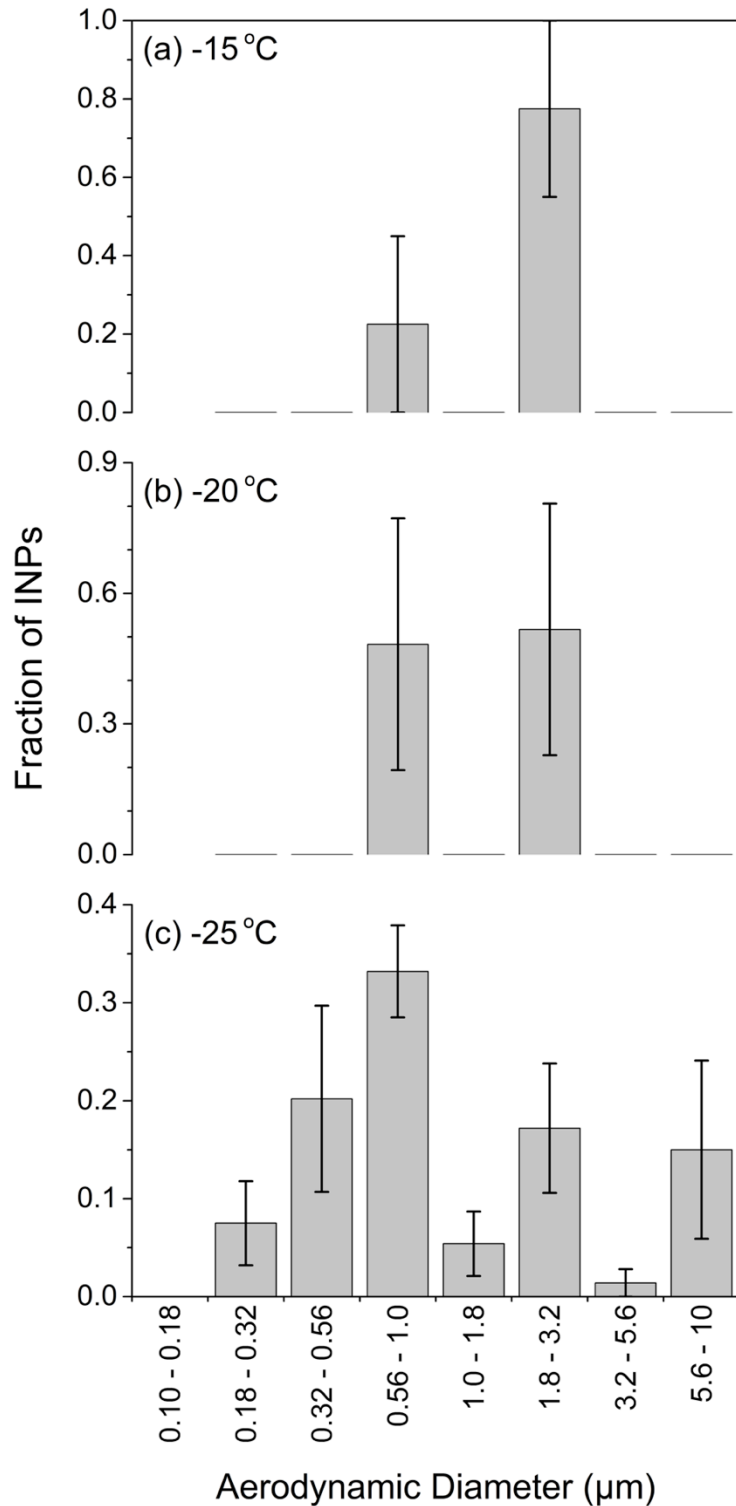


Figure S3. Mean INP size distributions at Whistler Mountain, BC, Canada at (a) -15 °C, (b) -20 °C, and (c) -25 °C. Here we report the fraction of INPs in each MOUDI size bin as the mean of all samples with uncertainty as the standard error of the mean. Number concentrations below 0.18 μm were not measured but plot axes are consistent with the other figures for easier comparison of the size distributions.

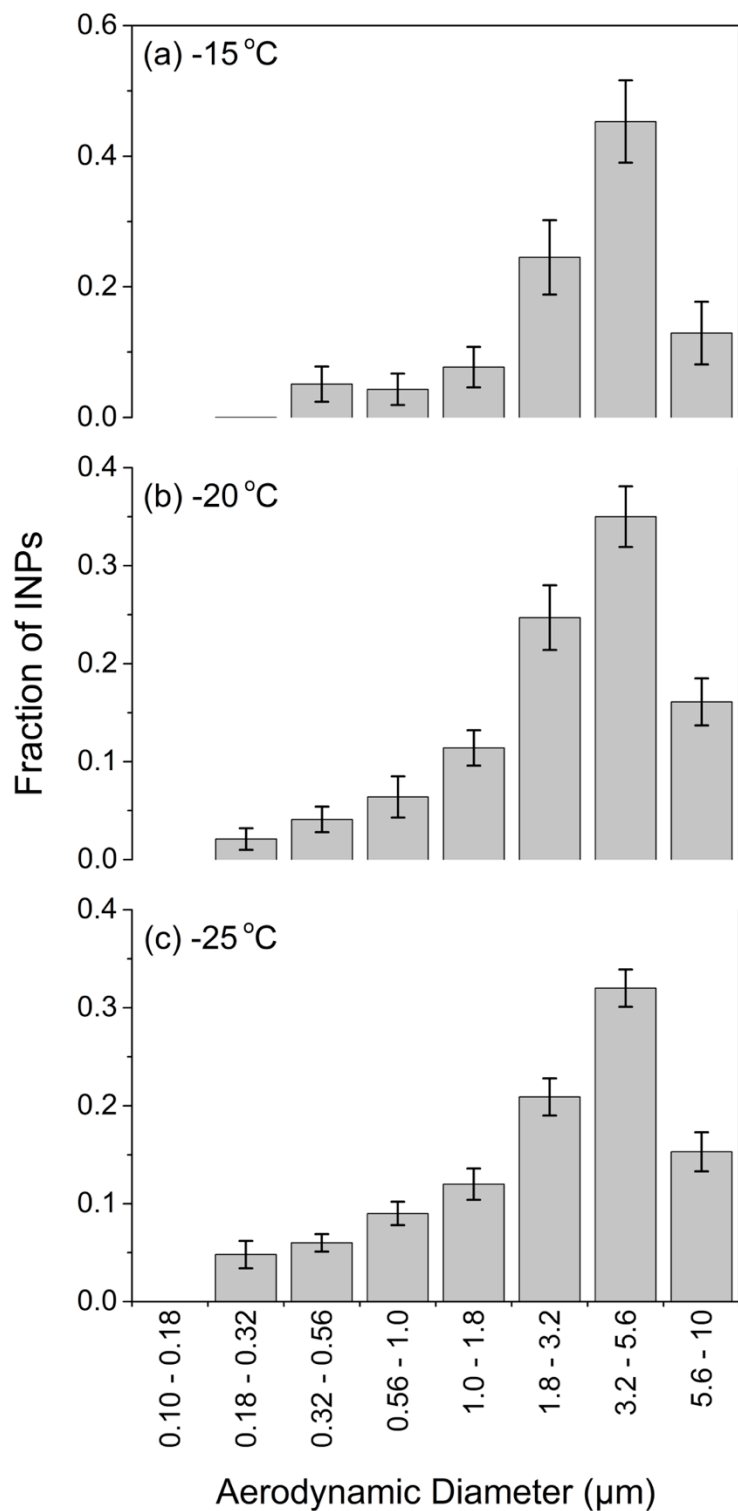


Figure S4. Mean INP size distributions at Amphitrite Point, BC, Canada at (a) -15 °C, (b) -20 °C, and (c) -25 °C. Here we report the fraction of INPs in each MOUDI size bin as the mean of all samples with uncertainty as the standard error of the mean. Number concentrations below 0.18 μm were not measured but plot axes are consistent with the other figures for easier comparison of the size distributions.

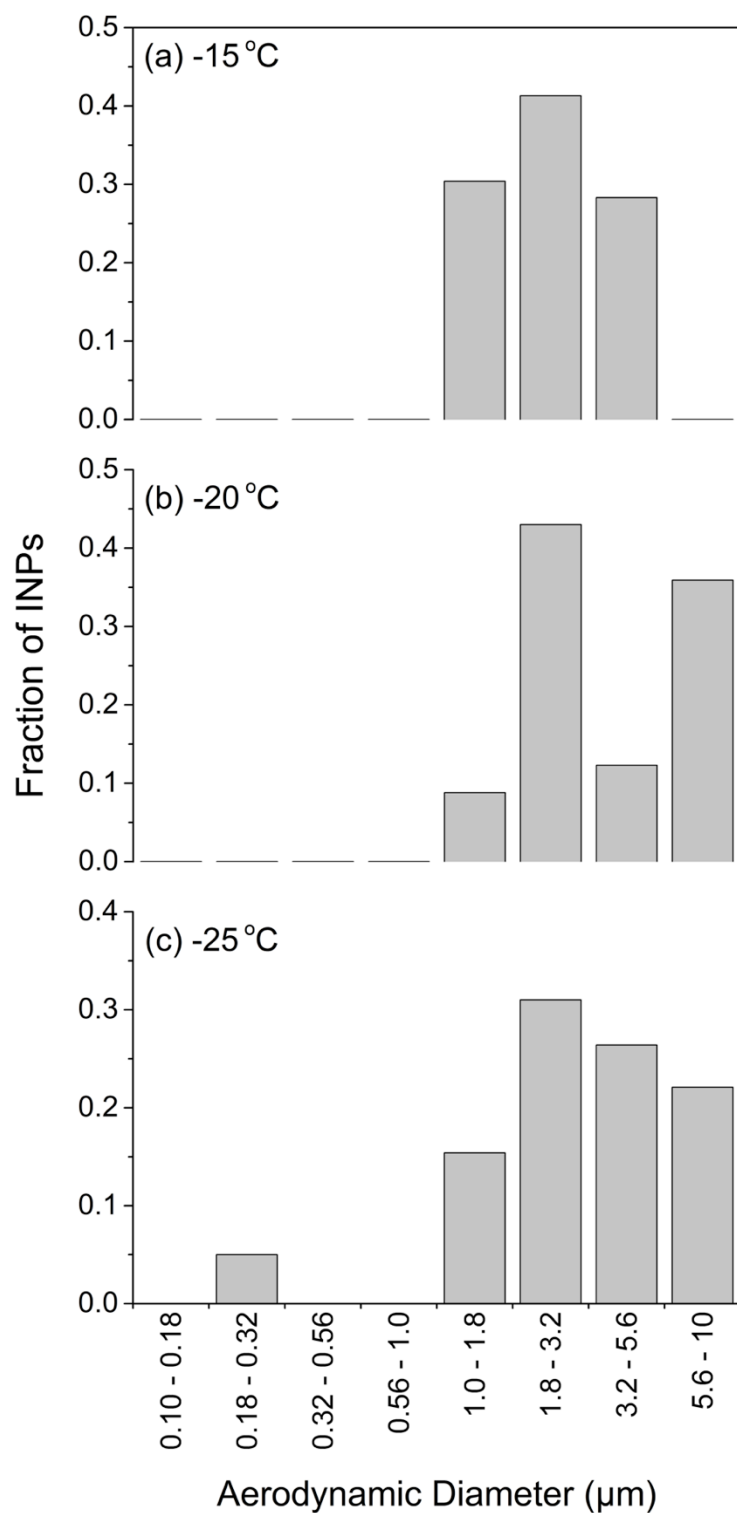


Figure S5. Mean INP size distributions at the Labrador Sea at (a) -15 °C, (b) -20 °C, and (c) -25 °C. Here we report the fraction of INPs in each MOUDI size bin as the mean of all samples with uncertainty as the standard error of the mean. As only one sample was collected at this location, no experimental uncertainty is reported.

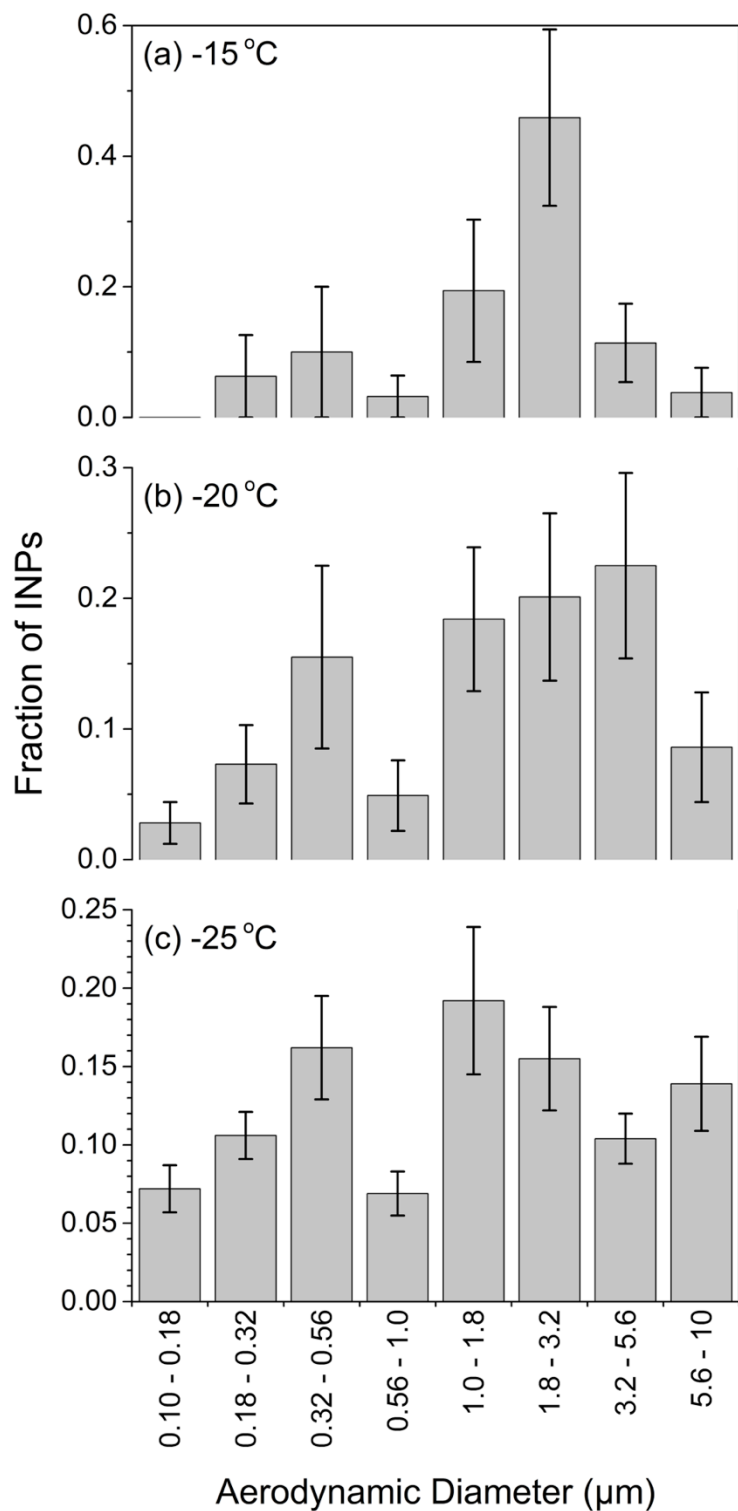


Figure S6. Mean INP size distributions at Saclay, France at (a) -15 $^{\circ}\text{C}$, (b) -20 $^{\circ}\text{C}$, and (c) -25 $^{\circ}\text{C}$. Here we report the fraction of INPs in each MOUDI size bin as the mean of all samples with uncertainty as the standard error of the mean.

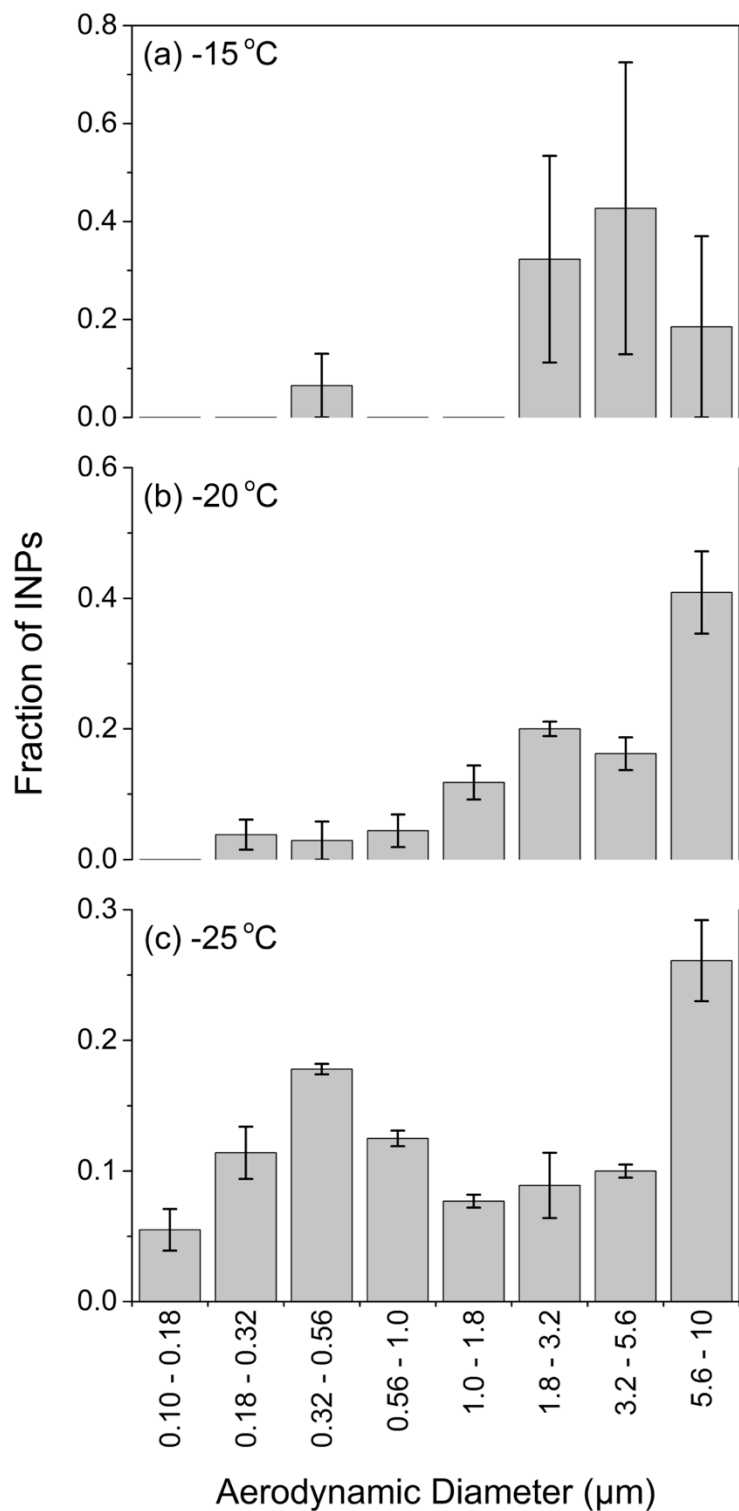


Figure S7. Mean INP size distributions at the UBC campus in BC, Canada at (a) -15 °C, (b) -20 °C, and (c) -25 °C. Here we report the fraction of INPs in each MOUDI size bin as the mean of all samples with uncertainty as the standard error of the mean.

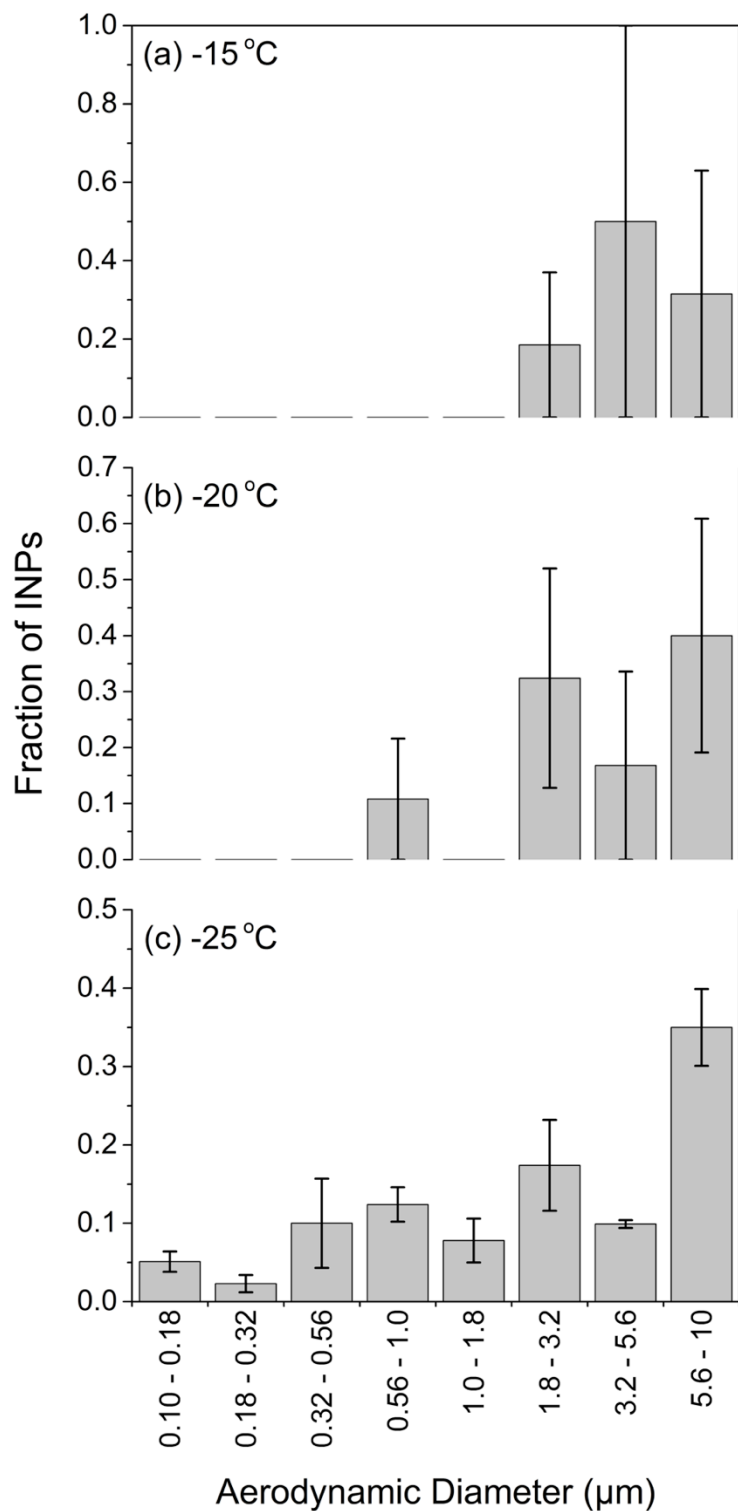


Figure S8. Mean INP size distributions at Colby, Kansas, USA at (a) -15 $^{\circ}\text{C}$, (b) -20 $^{\circ}\text{C}$, and (c) -25 $^{\circ}\text{C}$. Here we report the fraction of INPs in each MOUDI size bin as the mean of all samples with uncertainty as the standard error of the mean.